Journal of Materials Chemistry B

PAPER

View Article Online
View Journal | View Issue

Cite this: J. Mater. Chem. B, 2015, 3, 1667

Controlled release and corrosion protection by self-assembled colloidal particles electrodeposited onto magnesium alloys†

Jiadi Sun,[a] Ye Zhu,[a] Long Meng,[a] Wei Wei,[a] Yang Li,[a] Xiaoya Liu*[a] and Yufeng Zheng[b]

Received 11th October 2014
Accepted 1st January 2015

DOI: 10.1039/c4tb01683a

www.rsc.org/MaterialsB

We report a potential example of using surface functionalization to provide magnesium alloys (Mg–Ca) with controlled release and corrosion resistance properties. A key feature of this approach is to treat the Mg–Ca surfaces with nanoparticles *via* electrodeposition that can stably load and controllably release bioactive agents or drugs. These photo-cross-linkable and nano-scale particles were prepared by the self-assembly of an amphiphilic poly(γ-glutamic acid)-*g*-7-amino-4-methylcoumarin (γ-PGA-*g*-AMC) with encapsulation of a vitamin; moreover, the size and morphology of the resulting particles were studied. Fluorescence microscopy analysis indicated that Vm was effectively incorporated into the γ-PGA-*g*-AMC particles. Scanning electron microscopy (SEM) images showed that the colloidal particles could be uniformly electrodeposited on the Mg–Ca alloys. Fourier transform infrared spectroscopy (FTIR) and X-ray diffraction (XRD) analyses confirmed the successful anchoring of the particles. After the surface electrodeposition of self-assembled colloidal particles, the *in vitro* degradation results show that deposition of the particles was found to reduce the degradation rate of the magnesium alloys; moreover, the vitamin was controllably released for up to 20 days. Furthermore, the Mg–Ca substrate functionalized with colloidal particles containing a vitamin significantly promoted the attachment, proliferation and spread of NIH-3T3 normal cells. The entire strategy may be used in various medical devices to create coatings for improved biomedical performance.

1. Introduction

Magnesium alloys are potential materials for orthopedic implants and vascular stents due to their biocompatibility, as well as excellent physical and mechanical properties.[1,2] Because magnesium alloys are highly susceptible to electrochemical dissolution in physiological environments, various coatings have been used to reduce their degradation rate.[3] However, with the degradation of coating treated magnesium-based implant materials during their application, local cellular rejection and chronic inflammation may occur due to an adverse tissue reaction, especially during the early stages of implantation.[4,5] Therefore, interest in treating magnesium alloy surfaces with bioactive agents, such as phosphorylcholine or paclitaxel, has grown because they can mediate cellular responses or upregulate osteogenic activity in bone cells.[6,7] The key challenge in treating magnesium surfaces with bioactive agents is identifying a surface delivery system that can ensure efficient loading and controlled release of bioactive agents while maintaining their bioactivity and providing corrosion protection to the magnesium substrate.

Several surface treatments have been employed to produce sustained release of bioactive agents from magnesium surfaces. Xu *et al.*[8] fabricated micro-arc oxidation/poly-L-lactic acid and micro-arc oxidation/poly(lactide-*co*-glycolide) composite coatings on an AZ81 substrate to load and release paclitaxel drugs. Kumta *et al.*[9] developed layer-by-layer coatings of alginate and poly-L-lysine on alkali- or fluoride-pretreated AZ31 substrates to load fibronectin *via* chemical cross-linking. Although bioactive agents can readily be incorporated into or onto polymer coatings, the fabrication method, containing multiple steps and a low extent of interfacial adhesion between the polymer coating and the implant surface, can result in separation of the coating from the implant surfaces.

Recently, as controlled release systems for bioactive agents, hyaluronic acid-*g*-poly(lactic-*co*-glycolic acid) micelles encapsulating paclitaxel and polylysine were immobilized on cobalt–chromium alloys *via* layer-by-layer assembly.[10] Before this surface immobilization, the substrates needs to be treated with dopamine-derivatized heparin. Saltzman *et al.*[11,12] prepared PLGA nanoparticles loaded with dexamethasone or plasmid

[a]Key Laboratory of Food Colloids and Biotechnology, Ministry of Education, School of Chemical and Material Engineering, Jiangnan University, Wuxi, Jiangsu 214122, People's Republic of China. E-mail: lxy@jiangnan.edu.cn; Fax: +86-510-85917763; Tel: +86-510-85917763

[b]State Key Laboratory for Turbulence and Complex System and Department of Materials Science and Engineering, College of Engineering, Peking University, Beijing 100871, People's Republic of China

† Electronic supplementary information (ESI) available. See DOI: 10.1039/c4tb01683a

DNA using an oil-in-water (O/W) emulsion/solvent evaporation method, and then immobilized them onto a silicon oxide substrate through ionic interactions between the particles and metal oxide surfaces.[11,12] However, this surface treatment required additional pre-treatment of cationic poly(L-lysine) for particle immobilization, and the ionic interaction did not ensure stable adhesion of the nanoparticles on medical devices.

Herein, an electrodeposition technique was used to immobilize nanoparticles. This technique takes advantage of charged particles or molecules in solvents and is a low-temperature method suitable for manipulating a wide range of biomolecules and biological entities while maintaining their bioactivity. Another advantage of electrodeposition is its potential to produce uniform films on complex-shaped substrates.[13–16] The procedure is simple and uses inexpensive equipment. The coating formation can be controlled by the deposition conditions such as deposition time, bath concentration and applied potential. However, because magnesium alloys have high reaction rate with aqueous solutions in an applied electric field and the gas produced would prevent the formation of coatings. To immobilize nanoparticles on magnesium surfaces, we performed an electrodeposition process in ethanol solution, as reported in our previous study.[17]

In this study, we proposed a protective surface coating strategy based on the electrodeposition of self-assembled colloidal particles that stably load and release bioactive agents in a controlled manner. The overall fabrication procedure is illustrated in Fig. 1. Vitamin M (Vm), which is vital to all living beings and obtained entirely *via* the diet, was the selected bioactive agent template. Vm can promote cell differentiation and proliferation.[18,19] Therefore, a Vm-loaded surface may serve as a useful coating system for biological environments. The successful immobilization of colloidal particles onto magnesium surfaces and the phase compositions of the modified magnesium samples were examined. The degradation of the coated and uncoated magnesium alloys and the controlled release of Vm from the functionalized magnesium substrate were confirmed. The effect of Vm releasing particle coatings on the activity and morphology of NIH-3T3 normal cells was also estimated.

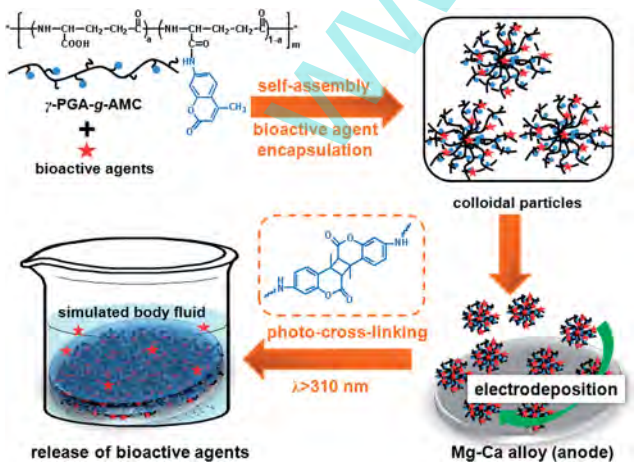

Fig. 1 Schematic illustration of controlled release coating fabrication using Vm loaded colloidal particles and electrodeposition.

2. Materials and methods

2.1 Materials

Poly(γ-glutamic acid) (γ-PGA, M_w = 200 000–500 000) was obtained from Wako Pure Chemical Industries Co., Ltd. (Osaka, Japan). 7-Amino-4-methylcoumarin (AMC), 1-ethyl-3-(3-dimethylaminopropyl)carbodiimide hydrochloride (EDC·HCl), 1-hydroxybenzotriazole (HOBt), fluorescein isothiocyanate (FITC), fluorescein diacetate (FDA), and vitamin M (Vm) were purchased from Aladdin Reagent Co., Ltd. (Shanghai, China). Dimethyl sulfoxide (DMSO), absolute ethanol, and triethylamine were acquired from Sinopharm Chemical Reagent Co., Ltd. (Shanghai, China). Dulbecco's modified Eagle's medium (DMEM: Gibco), fetal bovine serum (FBS: Hyclone), and penicillin streptomycin (Gibco) were purchased from Wuxi Trivd Biotechnology Inc. (Wuxi, China). All reagents and chemicals were used as received.

The Mg–Ca alloys (composition: 1 wt% Ca with the balance Mg, diameter 16 mm, 1.5 mm thick) were donated by Zheng *et al.*[20] The plates were ground using 1200# abrasive papers and ultrasonically cleaned with 10 mL ethanol and 10 mL acetone for 10 min.

2.2 Synthesis of γ-PGA-*g*-AMC copolymer

Photosensitive γ-PGA-*g*-AMC copolymers were synthesized as follows: a stirred solution of γ-PGA (1 mmol) in 40 mL DMSO was mixed with EDC·HCl (1 mmol) and HOBt (2 mmol) at room temperature. AMC (2 mmol) was then added to the reaction mixture and the reaction was maintained for 24 h. The resulting copolymer was isolated by dialysis using a membrane (molecular weight cut-off (MWCO): 14 000) against water before freeze-drying. The degree of AMC grafting was 20% as previously reported.[17]

2.3 Preparation of Vm loaded γ-PGA-*g*-AMC colloidal particles

Vm-loaded γ-PGA-*g*-AMC colloidal particles were prepared as follows: γ-PGA-*g*-AMC copolymers were dissolved in DMSO to form 5 mg mL^{-1} solutions with different initial Vm concentrations (0.3 mg mL^{-1}, 0.9 mg mL^{-1}, and 1.5 mg mL^{-1}). Then, twice the volume of absolute ethanol was added dropwise to yield translucent solutions. These solutions were dialyzed against ethanol for at least three days to remove DMSO and obtain stable colloidal particle solutions.

Loading amounts of Vm in the particles. To determine the contents of Vm loaded in the colloidal particles, Vm was dissolved in DMSO to make 5 mg L^{-1}, 8 mg L^{-1}, 10 mg L^{-1}, 12 mg L^{-1}, and 14 mg L^{-1} solutions. UV-vis spectra of the abovementioned solutions were recorded on a TU-1901 spectrophotometer in the wavelength range between 260 nm and 450 nm. Then, the standard curve equation was measured by fitting the absorbance readout at 281 nm. As Vm has poor solubility in ethanol, the unloaded Vm would be separated and precipitated during 1

h high-speed centrifugation at 10 000 rpm using a centrifuge (TG16-WS, China).[21] The supernatant liquid was removed and replaced with 5 mL DMSO. After ultrasonic dissolution for 10 min, the contents of unloaded Vm were determined by UV-vis measurement, and the absolute loading amounts (LA%) was calculated according to the following equation:[22]

$$\mathrm{LA}\% = \frac{\text{Total Vm} - \text{free Vm}}{\text{Total Vm}} \times 100\%$$

Particle sizing. The average size and size distribution of the particles were determined by dynamic light scattering (DLS) using ALV-5000/E DLS software (ALV/DLS/SLS-5000, Germany) with a 90° fixed scattering angle. The measurement was repeated three times for each sample. Moreover, all samples were filtered through 0.8 μm Milli-pore filters to remove dust before the measurements.

Atomic Force Microscopy (AFM). The morphologies of colloidal particles were measured using a CSPM3300 (Benyuan Co.) AFM with a vertical resolution of 0.1 nm and a horizontal resolution of 0.2 nm. The instrument was operated in the contact mode and the scanning range was set at 5.0 μm × 5.0 μm. The AFM measurement samples were prepared by casting a colloidal particle solution onto clean mica and drying it overnight in a constant-humidity oven at 30 °C. The measurement was repeated twice.

Visualization of Vm loading. FITC-labeled Vm was encapsulated into γ-PGA-*g*-AMC colloidal particles to visualize the Vm loading. As reported in previous studies,[23,24] FITC-labeled Vm synthesis was based on a reaction between the isothiocyanate groups in FITC (1 mmol) and the primary amino groups in Vm (1 mmol) in 30 mL DMSO for 10 h. The particles loaded with the FITC-labeled Vm were visualized using a Nikon 80i fluorescence microscope under a green filter.

2.4 Electrodeposition of the colloidal particles

A 30 mL particle solution was prepared in advance as the electrodeposition electrolyte, and the electrolyte concentration was 1.66 mg mL^{-1} γ-PGA-*g*-AMC loaded with 0.1 mg mL^{-1}, 0.3 mg mL^{-1}, and 0.5 mg mL^{-1} Vm. A small amount of triethylamine was added to adjust the pH of electrolyte (approximately 7.5) and deprotonate the –COOH groups around the particles. The Mg–Ca alloy and a Pt electrode were used as the working electrode (anode) and counter electrode (cathode), respectively. The particles were electrodeposited at 150 V for 30 minutes onto Mg–Ca alloy surfaces. The nanostructured surfaces were photo-cross-linked *via* exposure to UV light for 1.5 h on each side (the UV light was generated from a spot-curing system with a wavelength of 365 nm and a power of 200 W). Note that the samples were marked as Mg-CPVm$_{0.1}$, Mg-CPVm$_{0.3}$, and Mg-CPVm$_{0.5}$.

2.5 Electrodeposited particle characterization

Scanning electron microscopy (SEM, Hitachi S-4800, Japan) was used to determine the surface morphology of the coated samples. Images were acquired after sputtering gold at an operating voltage of 20 kV. The chemical composition of the electrodeposited particles was investigated using attenuated total reflectance Fourier transform infrared spectroscopy (ATR-FTIR, Nicolet 6700, USA) in diffuse reflectance mode. For each spectrum obtained, a total of 64 scans were accumulated at 4 cm^{-1} resolution in the wavenumber range of 500–4000 cm^{-1}. The phase composition of the prepared samples was studied by X-ray diffraction (XRD, D8, Germany). The data was collected from 3° to 90° with a step of 0.02° and a scanning rate of 4° min^{-1}. Contact angles were evaluated using a contact angle meter (OCA15EC, Germany). The results were measured at four different spots on the sample and the average contact angle value was adopted as the final result. The cross-section thickness of the obtained coating was studied using an ultra-depth of field three-dimensional microscope (VHX-1000C, Keyence, Hong Kong). Before taking this measurement, the coated samples were ground using 1200# abrasive papers to expose the cross-section parts.

Electrochemical tests were performed to evaluate the corrosion resistance of coated and bare Mg–Ca alloys in simulated body fluid (SBF) at 37 ± 0.5 °C.[25] Measurements were carried out using three-electrode cell. Coated and bare Mg–Ca samples were used as the working electrodes. A platinum plate and a saturated calomel electrode (SCE) were used as counter electrode and reference electrode, respectively. The scanning range was between −0.6 V and 0.6 V compared to open circuit potential with a rate of 1 mV s^{-1}.

An immersion test was carried out at different time points to monitor the degradation and the release of magnesium ions of coated and uncoated Mg–Ca samples. Three of each of the coated and uncoated samples were individually immersed in 100 ml SBF and then incubated at 37 °C for a total of 20 days. The release of magnesium ions from the samples was measured at five different time points (*i.e.* 2, 5, 7, 10, and 20 days) using an atomic absorption spectrophotometer (TAS-990NFG, China). A correlation between ion dissolution and time was subsequently established.

2.6 Controlled release of Vm

To determine the electrodeposited content of Vm on the Mg–Ca alloy surface, electrodeposited Mg-CPVm$_{0.1}$, Mg-CPVm$_{0.3}$, and Mg-CPVm$_{0.5}$ were immersed in 10 mL DMSO overnight at room temperature. Because Vm has high solubility in DMSO, the electrodeposited Vm would be completely released into the DMSO. Therefore, a UV-vis spectrophotometer (TU-1901, China) can be used to determine the amount of Vm electrodeposited on the Mg–Ca alloy surface for each sample and this value can be calculated using the equation described above.

In vitro release profiles for Vm from Mg–Ca substrates were examined in 100 mL SBF solution (pH = 7.4, 37 ± 0.5 °C). At predetermined time intervals, 1 mL of the medium was collected and replaced with an equal volume of fresh SBF medium. The amount of Vm released in the medium solution was investigated by UV-vis spectroscopy and quantified by the UV absorption intensity at 281 nm. All the samples were

prepared and tested in triplicate, and sample data are presented as the mean ± standard deviation (SD).

2.7 Cell culture

2.7.1 Indirect cell viability. Cell viability was examined using an MTT assay and NIH-3T3 normal cells (a mouse embryonic fibroblast cell line) with released extracts.[26] The extracts were collected from a controlled release experiment on day 2 and stored at 4 °C before testing. Before cell culturing, the extract solutions were filter sterilized through a 0.2 μm microporous membrane. The NIH-3T3 cells were cultured in 96-well plates at a density of 6×10^3 cells per well in 100 μL of Dulbecco's modified Eagle's medium (DMEM) supplemented with 10% fetal bovine serum (FBS) and 1% antibiotics at 37 °C in a humidified 5% CO_2 atmosphere. After 1 day of incubation to allow cell attachment, the culture medium was replaced with 50 μL DMEM and 50 μL of the released extract supplemented with 10% FBS and 1% antibiotics. The cells were then cultured for two more days. Moreover, the cells cultured with immersion extracts from a bare Mg–Ca alloy on day 2 served as controls.

The cell morphologies were visualized using an inverted optical microscope (CKX41, Olympus, Olympus America Inc.). For each sample, images were obtained from at least six different locations to create an overview of the cell attachments. Then, 10 μL of a 5 mg mL^{-1} MTT assay stock solution in PBS was added to each well of the plate. After incubating the cells for another 4 h, formazan was formed and dissolved in 100 μL DMSO per well. The absorbance was measured using a multimode detector (Tecan Infinite M200 PRO, Shanghai DoBio Biotech Co., Ltd) at a wavelength of 570 nm referenced to 630 nm. The cell viability was calculated using the following equation: cell viability (%) = $(OD_{sample}/OD_{control}) \times 100\%$.

2.7.2 Direct cell adhesion. Before the measurements, bare Mg–Ca alloys were sterilized under ultraviolet (UV) light for 1.5 h on each side and coated samples were sterilized using UV light during the cross-linking process. NIH-3T3 normal cells were seeded onto each sample in 24-well tissue culture plates at a density of 6×10^3 cells per well in 500 μL of Dulbecco's modified Eagle's medium (DMEM) containing 10% fetal bovine serum (FBS) and 1% antibiotics at 37 °C in a humidified 5% CO_2 atmosphere. The cells were cultured for 24 h, and then 1 μL of 5 mg mL^{-1} fluorescein diacetate (FDA)–acetone solution was added to each well. The cells were cultured for another 15 min to stain. The seeded samples were then rinsed twice with sterile PBS and cell images were captured using a fluorescence microscope under a green filter (Nikon 80i, Japan). At least six different locations were imaged for each sample to view the cell attachments.

2.7.3 Statistical analysis. All biological experiments were performed independently in quadruplicate ($n = 4$), and three replicates were tested for each experimental point unless otherwise specified. The data were expressed as the mean ± standard deviation (SD). The statistical analysis was based on a one-way analysis of variance using Origin 8.6 software, and a p value less than 0.05 was considered to be statistically significant. Note that only relevant statistical relationships are denoted in the figures.

3. Results and discussion

3.1 Characteristics of Vm loaded γ-PGA-*g*-AMC colloidal particles

There are abundant free carboxyl groups in the linear γ-PGA-*g*-AMC copolymer chains. Vm contains two carboxyl groups and a secondary amino group. When Vm is added to the γ-PGA-*g*-AMC solution, it is adsorbed onto the γ-PGA-*g*-AMC main chain *via* hydrogen bonding and electrostatic interactions. With the addition of ethanol, γ-PGA-*g*-AMC copolymer chains start aggregating and forming self-assembled colloidal particles. During this process, Vm is encapsulated into these particles.

The size and morphology of the resulting particles loaded with 0.1 mg mL^{-1} Vm were determined by DLS and AFM. The results are shown in Fig. 2: the mean hydrodynamic radius calculated by DLS is 149.2 nm, and the size has a moderate distribution (Fig. 2A). The dry particle diameter is almost 123 nm as measured by AFM (Fig. 2B). Compared to the size (R_h = 149.2 nm) determined by DLS, the AFM results indicated a smaller size because of shrinkage of the particles in the dried state after removing the absorbed solvent. Since self-assembly is a dynamic equilibrium process, Vm concentration can affect the formation of colloidal particles. Thus, the R_h values for colloidal

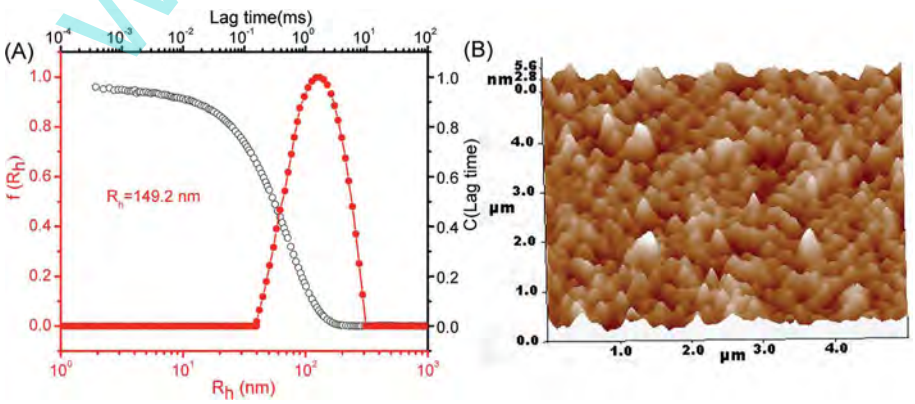

Fig. 2 Hydrodynamic radius distribution (A) and AFM image (B) of 1.66 mg mL^{-1} colloidal particles with 0.1 mg mL^{-1} Vm encapsulation.

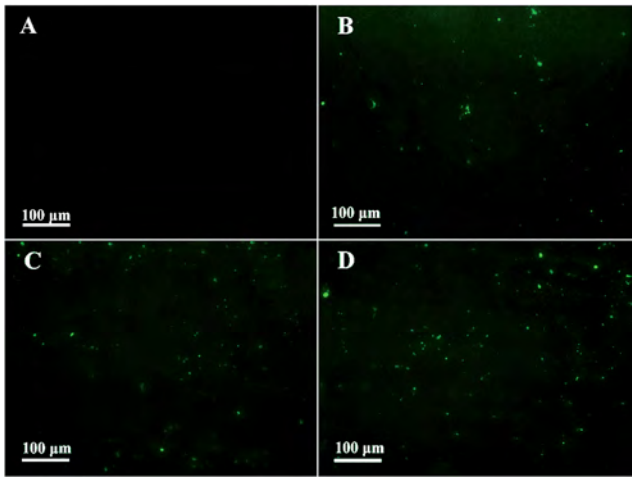

Fig. 3 Fluorescence microscopy images of bare γ-PGA-*g*-AMC colloidal particles (A) and samples with encapsulated FITC-labeled Vm at concentrations of 0.1 mg mL^{-1} (B), 0.3 mg mL^{-1} (C), and 0.5 mg mL^{-1} (D).

particles loaded with different concentrations of Vm were studied. As shown in Fig. S1,† the average R_h increased from 149.2 nm to 210.1 nm with the incorporation of Vm content ranging from 0.1 mg mL^{-1} to 0.5 mg mL^{-1}, because increase in the Vm concentration can increase the compatibilization effect of the colloidal particles. In addition, the absolute loading amounts for all particle samples were 100% as determined using UV-vis measurement and a standard curve of Vm (as shown in Fig. S2†). The relatively high loading amounts of Vm for different samples may be attributed to the strong interaction between Vm and γ-PGA-*g*-AMC. These results indicate Vm loaded γ-PGA-*g*-AMC colloidal particles can be obtained *via* self-assembly.

To visualize the incorporation of Vm into the γ-PGA-*g*-AMC colloidal particles, Vm was labeled with a green fluorescent FITC and loaded into the particles. The FITC-labeled Vm structure was determined by the fluorescence spectra (as shown in Fig. S3†). Particle solutions were dispensed onto glass slides, washed three times with distilled water, and visualized using fluorescence microscopy. As shown in Fig. 3, compared to bare γ-PGA-*g*-AMC colloidal particles (A), those loaded with Vm exhibit obvious FITC-fluorescence (B, C, and D). Moreover, the density of fluorescent spots increases with increasing Vm concentration, suggesting that Vm was efficiently loaded into the γ-PGA-*g*-AMC colloidal particles.

3.2 Electrodeposition of colloidal particles

Electrodeposition is attracting increasing attention in biomedical field due to its relatively low cost, simplicity of the required equipment, ability to process at room temperature and potential to produce a wide range of coatings on complex structures.[27] For surface immobilization, 1.66 mg mL^{-1} particle solutions with 0.1 mg mL^{-1}, 0.3 mg mL^{-1}, and 0.5 mg mL^{-1} Vm loadings were deposited on Mg–Ca substrates and denoted as Mg-$CPVm_{0.1}$, Mg-$CPVm_{0.3}$, and Mg-$CPVm_{0.5}$, respectively. As shown in Fig. 4 (high magnification) and Fig. S4 in the ESI† (low magnification), SEM indicates that Vm-loaded colloidal particles were stably electrodeposited onto the Mg–Ca surfaces (A1, B1, and C1). The particles form uniform films with some colloidal particles, which is clearly visible at high magnification. Because the particles contain coumarin groups, they can photochemically dimerize on the electrodeposited surfaces *via* direct UV irradiation (λ > 310 nm). After 1.5 h of UV exposure, the coated surfaces (A2, B2, and C2) became much denser and smoother due to photo-cross-linking of the particles. This improvement can ensure good mechanical stability and barrier properties of the resulting coating system.[28–30]

To verify the chemical composition of the electrodeposited particles, the FTIR spectra of the native γ-PGA-*g*-AMC copolymer, Vm, and immobilized colloidal particles for Mg-$CPVm_{0.1}$, Mg-$CPVm_{0.3}$, and Mg-$CPVm_{0.5}$ were obtained. X-ray diffraction was used to determine the phase composition of different samples, and the results are shown in Fig. 5. The peaks at 3540.87 cm^{-1}, 3410.93 cm^{-1}, and 3318.30 cm^{-1} in the Vm FTIR spectrum are due to the stretching vibrations of $-NH_2$, –NH–, and –OH groups, respectively. The band observed at 3306.97 cm^{-1} is related to –OH stretching vibrations in the –COOH groups in γ-PGA-*g*-AMC main chains. All of these characteristic peaks are present in the electrodeposited particle spectra, indicating the successful incorporation of Vm into γ-PGA-*g*-AMC particles. The XRD patterns of bare and coated alloys are shown in Fig. 5B. It is evident that the intensity of the Mg phase

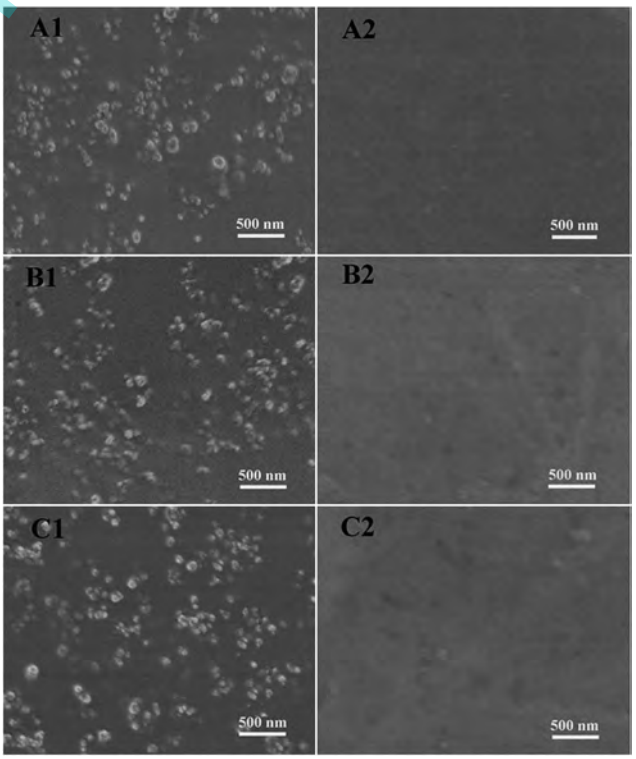

Fig. 4 SEM images of the coated samples before (A1, B1 and C1) and after (A2, B2 and C2) photo-cross-linking, (A) Mg-$CPVm_{0.1}$, (B) Mg-$CPVm_{0.3}$, (C) Mg-$CPVm_{0.5}$. The UV irradiation time is 1.5 h using a spot curing system (200 W, 365 nm), magnification: 30 000×.

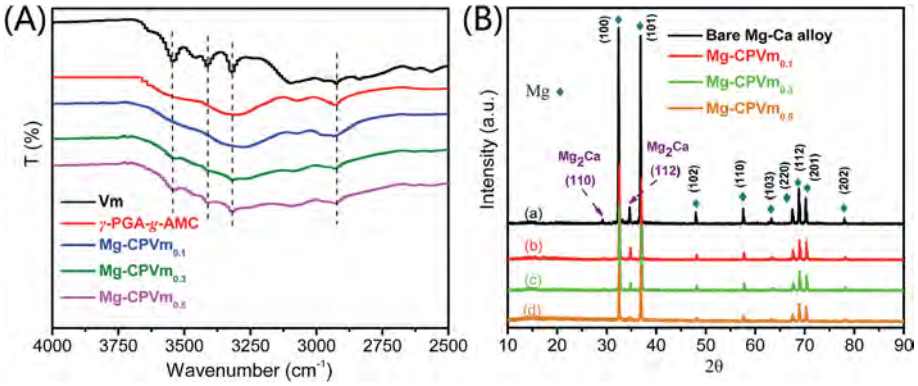

Fig. 5 ATR-FTIR spectra (A) and XRD patterns (B) for different samples.

of bare substrate is very strong. After electrodepositing colloidal particles, the intensity of the Mg phase of the coated samples decreased. These results indicate that Vm incorporating colloidal particles have been electrodeposited onto the Mg–Ca alloy surfaces.

3.3 *In vitro* degradation and corrosion

Potentiodynamic polarisation was conducted to assess the general protective characteristics of the particle-modified surfaces in relation to a standard Mg–Ca alloy. Generally, the cathodic polarization curves are assumed to represent cathodic hydrogen evolution *via* water reduction, whereas the anodic polarization curves represent the dissolution or destruction behaviors of protective coating.[31] This means that more positive the corrosion potential and lower the polarization current, the better the corrosion resistance. As seen in Fig. 6A and Table 1 in the ESI,† the Mg–Ca alloy displayed a corrosion potential (E_{corr}) of −1.80 V and a corrosion current density (i_{corr}) of 8.71×10^{-4} A cm^{-2}. After electrodeposition, E_{corr} increased and i_{corr} decreased: the E_{corr} values increased to −1.49 V for Mg-CPVm$_{0.1}$, −1.45 V for Mg-CPVm$_{0.3}$, and −1.42 V for Mg-CPVm$_{0.5}$. Compared to the Mg–Ca alloy, the shift of E_{corr} in the positive direction can be attributed to the protective properties of particle-modified surfaces formed on the substrates. i_{corr} decreased to 1.85×10^{-4}, 8.63×10^{-5} and 7.94×10^{-5} A cm^{-2} for Mg-CPVm$_{0.1}$, Mg-CPVm$_{0.3}$ and Mg-CPVm$_{0.5}$, respectively. These results indicate that all the coated samples exhibit better protective function as reflected in their more positive E_{corr} and lower i_{corr}.

Since magnesium substrates are highly susceptible to electrochemical dissolution in physiological environments, the degradation property of each sample was estimated.[32] The changes in Mg^{2+} ion concentration in the immersion medium over time during the degradation process of different samples are presented in Fig. 6B. As shown in the results, the amount of Mg^{2+} released from the bare Mg–Ca substrate was much higher than that released from the Mg-CPVm$_{0.1}$, Mg-CPVm$_{0.3}$, and Mg-CPVm$_{0.5}$ samples. More importantly, compared with that of Mg-CPVm$_{0.1}$ and Mg-CPVm$_{0.3}$, the release of Mg^{2+} ions from Mg-CPVm$_{0.5}$ is much lower. Because Vm contains two aromatic portions, higher Vm amounts in the particles can increase the hydrophobicity of the resulting coating, as shown in Fig. S5A.† In addition, an increase in the Vm amount can also increase the solid content of the electrolyte used in the electrodeposition process, thus increasing the thickness of the resulting coating. Note that the data are shown in Fig. S5B.† Therefore, the decrease in the amount of Mg^{2+} ion released from Mg-CPVm$_{0.1}$ to Mg-CPVm$_{0.5}$ is understandable, because strong hydrophobicity and greater thickness of the surface coating can slow the

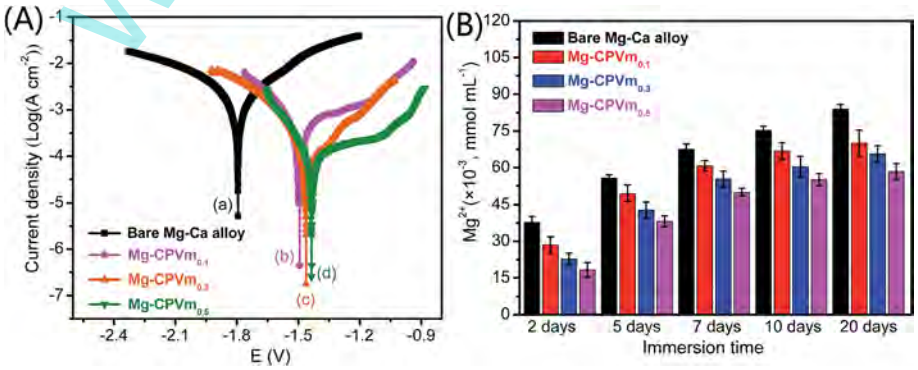

Fig. 6 Polarization curves of bare Mg–Ca alloy and coated samples in 30 mL SBF, pH = 7.4 (A), magnesium ion release from bare Mg–Ca alloy and coated samples in SBF medium over a period of 20 days (B).

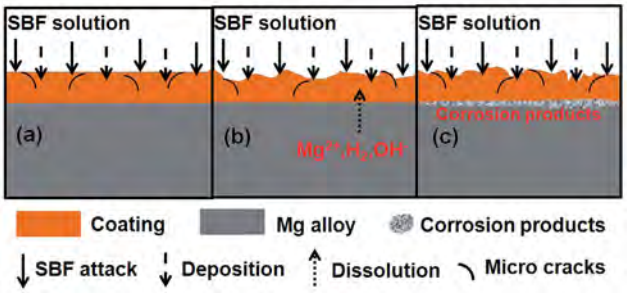

Fig. 7 Proposed pictorial model to explain degradation and corrosion mechanism of biological coating on magnesium by immersion in SBF at 37 °C, process of degradation of the coating (a), localized corrosion of the substrate (b), and the formation of corrosion products (c).

degradation rate of the magnesium alloy. These results clearly demonstrate that the deposited coating can provide a corrosion protection barrier for the underlying Mg–Ca alloy.

The electrochemical and immersion tests demonstrate that the coated Mg–Ca samples have lower degradation and corrosion rates compared to the bare Mg–Ca alloy. The main protective mechanism of the coating can be summarized as follows: degradation of the coating (a), localized corrosion of the substrate (b), and the formation of corrosion products (c), which are schematically illustrated in Fig. 7. During the early immersion period, the Mg–Ca substrate and SBF corrosive solution were physically isolated by coating. Since the coating contained many hydrophilic groups, the surface of the coating would swell and produce micro-cracks under erosion by the SBF solution. With an extension of immersion time, the SBF corrosive solution then permeated into the coating and corroded the Mg–Ca substrate with the release of Mg^{2+} ions, OH^- ions, and H_2 gas. Thus, the release behavior of the substrate resulted in more and more cracks in the coating with increasing immersion time, which can accelerate the degradation rate of protective coating. When the OH^- around the substrate achieves a higher concentration, corrosion products were formed due to a reaction between OH^- and calcium, magnesium and phosphate ions. At this juncture, the coating can slow the diffusion of corrosion products to the SBF solution, thus decreasing the corrosion rate of the underlying magnesium alloy.[33–36]

3.4 Vm loading and controlled release from Mg–Ca substrates

The amount of Vm loaded onto Mg–Ca substrates can be controlled by adjusting the concentration of the incorporated Vm. For the Vm feed contents of 3 mg, 9 mg, and 15 mg, the loading amounts of Vm on the particle-immobilized Mg–Ca surfaces are approximately 2.437 mg, 5.101 mg, and 8.558 mg, respectively, as calculated from the standard curve determined by UV-vis measurements.

To investigate the controlled release property of the modified Mg–Ca surfaces, *in vitro* release experiments were conducted in an SBF environment, and a standard curve for Vm in an aqueous environment was obtained using a TU-1901 spectrophotometer at wavelengths between 200 nm and 450 nm (as

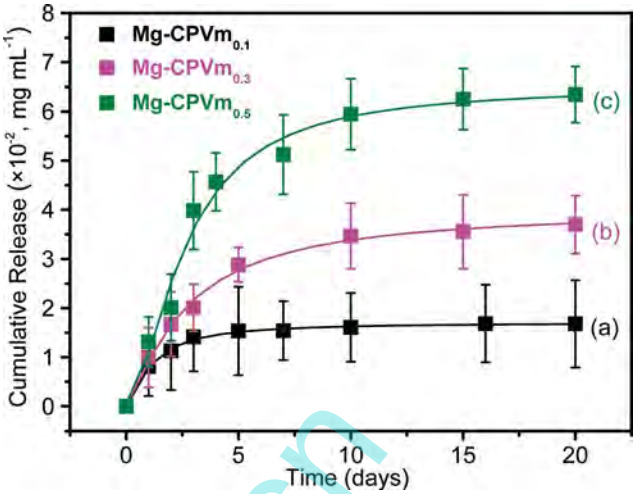

Fig. 8 Cumulative *in vitro* release profiles for Vm from the coated samples in 100 mL SBF at 37 ± 0.5 °C and pH = 7.4, Mg-CPVm$_{0.1}$ (a), Mg-CPVm$_{0.3}$ (b), and Mg-CPVm$_{0.5}$ (c). Data were expressed as mean ± SD (n = 3).

shown in Fig. S6†). Before these tests, all samples were subjected to UV irradiation in order to improve the mechanical stability of the immobilized particles. Fig. 8 shows that Vm was released for up to 20 days from Mg-CPVm$_{0.1}$, Mg-CPVm$_{0.3}$, and Mg-CPVm$_{0.5}$, respectively. The quantity of Vm released from the Mg–Ca substrates is controlled by adjusting the Vm load and the degradation process of the resulting sample, where higher Vm loads and rapid degradation rates result in higher amounts released.[37] After 20 days, the cumulative quantity of Vm released from Mg-CPVm$_{0.1}$, Mg-CPVm$_{0.3}$, and Mg-CPVm$_{0.5}$ was 1.678 mg, 3.698 mg, and 6.344 mg, respectively. Because the substrates can react with water and cause damage to the coated surfaces, there is a burst release for each sample. In addition, these results also indicate that nanostructured coatings, similar to nanogels,[38] can protect loaded Vm from decomposition in the presence of heat, UV light, or oxygen, to release naturally structured Vm.

The release mechanism of Vm from the coated sample is tightly dependent on the degradation and corrosion of the coating and the underlying Mg–Ca substrate. Initially, the surface of the coating would swell and some cracks were produced with erosion by SBF solution at 37 °C. At this point, Vm was released by diffusion through the fractures produced by the swelling and erosion processes. With an increase in immersion time, the SBF solution permeated into the coating and corroded the Mg–Ca substrate with the release of different ions. This release behavior of the Mg–Ca substrate produced more cracks and channels in the coating and increased the degradation rate of the protective coating, thus accelerating the release rate of the Vm entrapped in the coating.[8,39–41]

3.5 Cell viability assay

3.5.1 Indirect cell viability. The cell morphology of NIH-3T3 was examined by optical microscopy. The results are shown in Fig. 9(A–D). After two days of cell culturing, there were evident

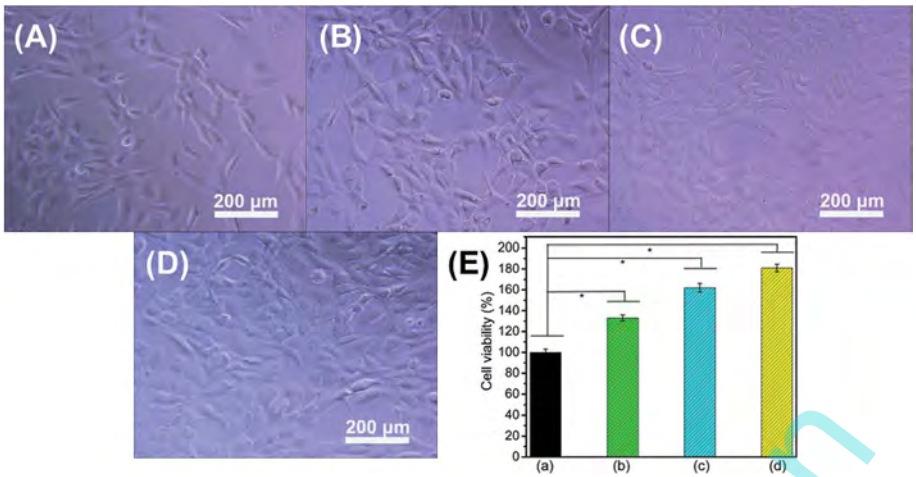

Fig. 9 Optical microscopy images of NIH-3T3 cells after incubating for two days with extracts released from bare Mg–Ca alloy (A, control group), Mg-CPVm$_{0.1}$ (B), Mg-CPVm$_{0.3}$ (C), and Mg-CPVm$_{0.5}$ (D). Cell viability of NIH-3T3 for different samples (E): bare Mg–Ca alloy (a), Mg-CPVm$_{0.1}$ (b), Mg-CPVm$_{0.3}$ (c), and Mg-CPVm$_{0.5}$ (d). Data were expressed as mean ± SD ($n = 4$). Statistically significant differences exhibited *$p < 0.05$ *vs.* control.

cell growth differences between the extracts released from Mg-CPVm$_{0.1}$, Mg-CPVm$_{0.3}$, Mg-CPVm$_{0.5}$, and the bare Mg–Ca alloy. The cells cultured with extracts released from Vm-releasing surfaces exhibit more confluence, have good cell spread and maintain their overall orientation, in contrast to that observed for bare substrate. This observed cell morphology suggests that the extracts from different samples are well tolerated by NIH-3T3 cells, and higher NIH-3T3 cell densities are obtained using particle-treated Mg–Ca surfaces with controlled release properties.

The cell viability of the different samples was evaluated by an MTT assay using NIH-3T3 cells. The MTT assay is based on the ability of a mitochondrial dehydrogenation enzyme in a viable cell to cleave the tetrazolium rings of pale-yellow MTT and form dark-blue formazan crystals.[42] Fig. 8E shows the cell viability after incubating for two days with the extracts released from bare Mg–Ca alloy, Mg-CPVm$_{0.1}$, Mg-CPVm$_{0.3}$, and Mg-CPVm$_{0.5}$, respectively. The results demonstrate that high cell viabilities ranging from 133% to 181% were obtained from the Mg-CPVm$_{0.1}$, Mg-CPVm$_{0.3}$, and Mg-CPVm$_{0.5}$ extracts, revealing improved cytocompatibility of the particle-treated surface. As reported in a previous study,[43] the viability of cells grown in an extract is strongly correlated with the product ingredients of the sample. The main ingredients of the immersion extracts used in the cell experiments are Mg^{2+} ion, OH^- and released Vm. Since Vm can promote cell growth and proliferation, higher Vm concentrations would contribute to cell viability. However, higher ion contents in the medium would damage the cellular ion balance, cellular metabolism, and other features.[44,45] As shown in Fig. S7,† the Vm contents in the extracts released from bare Mg–Ca, Mg-CPVm$_{0.1}$, Mg-CPVm$_{0.3}$, and Mg-CPVm$_{0.5}$ on day 2 were 0 mg mL^{-1}, 5.5×10^{-3} mg mL^{-1}, 8.0×10^{-3} mg mL^{-1}, and 1.0×10^{-2} mg mL^{-1}, respectively. The contents of magnesium ions were 18.9×10^{-3} mmol mL^{-1}, 14.2×10^{-3} mmol mL^{-1}, 11.3×10^{-3} mmol mL^{-1}, and 9.1×10^{-3} mmol mL^{-1}, respectively, and similar trends in pH were observed for the samples (data not shown). Therefore, the cell viabilities increased significantly from the extracts released from Mg-CPVm$_{0.1}$ to those from Mg-CPVm$_{0.5}$.

3.5.2 Direct cell attachment. Good cell adhesion properties are accepted to favor cell survival. To determine the attachment of NIH-3T3 cells to bare and coated Mg–Ca alloy samples, these cells were seeded onto the surfaces of different samples. Fig. 10 shows the morphology of NIH-3T3 cells after culturing for 24 h on bare Mg–Ca alloy, Mg-CPVm$_{0.1}$, Mg-CPVm$_{0.3}$, and Mg-CPVm$_{0.5}$, respectively. As shown in the results, Mg-CPVm$_{0.1}$, Mg-CPVm$_{0.3}$, and Mg-CPVm$_{0.5}$ display good cell focal adhesion and spread compared to bare Mg–Ca alloy. Most of the NIH-3T3 cells on the bare Mg–Ca alloy surface failed to spread well, although they appeared to attach to the sample surface. This phenomenon occurred because magnesium alloys are chemically active and can easily react with a cell culturing medium, which affects

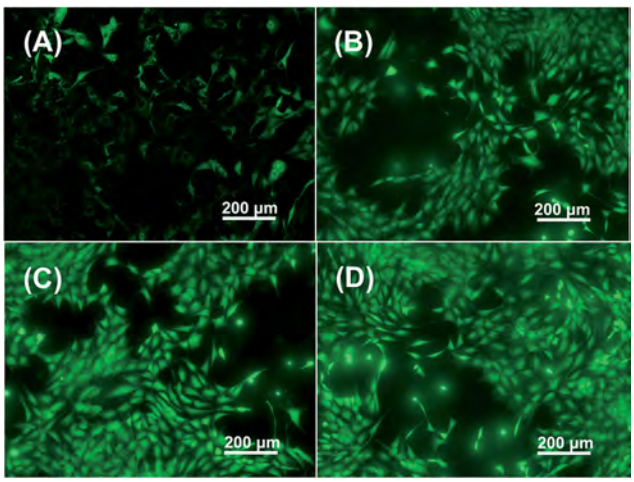

Fig. 10 Fluorescent images of NIH-3T3 cells after culturing for 24 h on bare Mg–Ca alloy (A), Mg-CPVm$_{0.1}$ (B), Mg-CPVm$_{0.3}$ (C), and Mg-CPVm$_{0.5}$ (D).

cell attachment and spread.[46] However, the cells attached to the Mg-CPVm$_{0.1}$, Mg-CPVm$_{0.3}$, and Mg-CPVm$_{0.5}$ samples exhibit more evident filopodia and flattened membranes. Because the Mg–Ca surface coatings avoid interfacial contact between the cells and the chemically active Mg–Ca alloy, the NIH-3T3 cells can adhere to the coating surface and grow. These results indicate that the Vm-releasing Mg–Ca alloy surfaces improve cell adhesion and spread.

4. Conclusions

In this study, we developed a novel and efficient approach to generate nanostructured surfaces based on the electrodeposition of self-assembled colloidal particles that may serve as surface protection and release systems for various medical devices. These particles not only feature good UV responses but also allow Vm incorporation when prepared *via* self-assembly of a γ-PGA-*g*-AMC copolymer. The self-assembled colloidal particles were uniformly immobilized on the Mg–Ca alloy surfaces through a simple electrodeposition process. The homogeneity and sealability of the electrodeposited particles on the Mg–Ca surface were readily modulated *via* further UV irradiation and the particle-modified surface can reduce the degradation rate of the Mg–Ca substrate. More importantly, the incorporated Vm can be released in a controlled manner. Moreover, the Vm-releasing Mg–Ca alloy surfaces could provide an environment that promoted NIH-3T3 cell activity. This strategy, which combines the advantages of self-assembled colloidal particles and electrodeposition, may be used as a platform for surface controlled release systems for various medical devices such as stents and dental and orthopedic implants.

Acknowledgements

This study was supported by the National Natural Science Foundation of China (NSFC) (under Grants nos 20974041, 21174056), the Fundamental Research Funds for the Central Universities (JUSRP 51305A), MOE & SAFEA for the 111 Project (B13025), and the funds from the Jiangsu postgraduate scientific research and innovation plan project (under Grant no. KYLX_1128).

References

1 T. S. N. Sankara Narayanan, I. S. Park and M. H. Lee, *J. Mater. Chem. B*, 2014, **2**, 3365–3382.
2 Y. F. Zheng, X. N. Gu, N. Li and W. R. Zhou, *Mater. China*, 2011, **30**(4), 30–43.
3 H. Hornberger, S. Virtanen and A. R. Boccaccini, *Acta Biomater.*, 2012, **8**, 2442–2455.
4 F. Witte, J. Fischer, J. Nellesen, H. A. Crostack, V. K. Pisch, F. Beckmann and H. Windhagen, *Biomaterials*, 2006, **27**, 1013–1018.
5 W. D. Mueller, M. L. Nascimento and M. F. L. Mele, *Acta Biomater.*, 2010, **6**, 1749–1755.
6 S. H. Ye, Y. S. Jang, Y. H. Yun, V. Shankarraman, J. R. Woolley, Y. Hong, L. J. Gamble, K. Ishihara and W. R. Wagner, *Langmuir*, 2013, **29**(26), 8320–8327.
7 P. Lu, Y. Liu, M. Q. Guo, H. D. Fang and X. H. Xu, *Mater. Sci. Eng., C*, 2011, **31**(7), 1285–1289.
8 P. Lu, H. Fan, Y. Liu, L. Cao, X. Wu and X. Xu, *Colloids Surf., B*, 2011, **83**(1), 23–28.
9 S. Kunjukunju, A. Roy, M. Ramanathan, B. Lee, J. E. Candiello and P. N. Kumta, *Acta Biomater.*, 2013, **9**(10), 8690–8703.
10 T. G. Kim, H. Lee, Y. Jang and T. G. Park, *Biomacromolecules*, 2009, **10**, 1532–1539.
11 C. T. Lo, P. R. Van Tassel and W. M. Saltzman, *Biomaterials*, 2009, **30**(28), 4889–4897.
12 C. T. Lo, P. R. Van Tassel and W. M. Saltzman, *Biomaterials*, 2010, **31**(13), 3631–3642.
13 R. Fernandes, L. Q. Wu, L. H. Chen, H. Yi, G. W. Rubloff, R. Ghodssi, W. E. Bentley and G. F. Payne, *Langmuir*, 2003, **19**, 4058–4062.
14 X. L. Luo and X. T. Cui, *Acta Biomater.*, 2011, **7**, 441–446.
15 R. Ma, R. F. Epand and I. Zhitomirsky, *Colloids Surf., B*, 2010, **77**, 279–285.
16 S. Seuss and A. R. Boccaccini, *Biomacromolecules*, 2013, **14**, 3355–3369.
17 J. D. Sun, X. Y. Liu, L. Meng, W. Wei and Y. F. Zheng, *Langmuir*, 2014, **30**, 11002–11010.
18 M. J. Akhtar, M. A. Khan and I. Ahmad, *J. Pharm. Biomed. Anal.*, 1999, **19**(3–4), 269–275.
19 M. K. Off, A. E. Steindal, A. C. Porojnicu, A. Juzeniene, A. Vorobey, A. Johnsson and J. Moan, *J. Photochem. Photobiol., B*, 2005, **80**(1), 47–55.
20 Z. J. Li, X. N. Gu, S. Q. Lou and Y. F. Zheng, *Biomaterials*, 2008, **29**, 1329–1344.
21 B. Chimanuka, M. Gabriëls, M. R. Detaevernier and J. A. Plaizier-Vercammen, *J. Pharm. Biomed. Anal.*, 2002, **28**, 13–22.
22 L. Liu, L. Jiang, G. K. Xu, C. Ma, X. G. Yang and J. M. Ya, *J. Mater. Chem. B*, 2014, **2**, 7596–7604.
23 Y. H. Lin, C. K. Chung, C. T. Chen, H. F. Liang, S. C. Chen and H. W. Sung, *Biomacromolecules*, 2005, **6**(2), 1104–1112.
24 Y. H. Lin, F. L. Mi, C. T. Chen, W. C. Chang, S. F. Peng, H. F. Liang and H. W. Sung, *Biomacromolecules*, 2007, **8**(1), 146–152.
25 T. Kokubo and H. Takadama, *Biomaterials*, 2006, **27**(15), 2907–2915.
26 Y. Zhao, M. I. Jamesh, W. K. Li, G. S. Wu, C. X. Wang, Y. F. Zheng, K. W. K. Yeung and P. K. Chu, *Acta Biomater.*, 2014, **10**, 544–556.
27 O. D. Velev and K. H. Bhatt, *Soft Matter*, 2006, **2**, 738–750.
28 R. Baskar, D. Kesavan, M. Gopiraman and K. Subramanian, *RSC Adv.*, 2013, **3**, 17039–17047.
29 R. Baskar, D. Kesavan, M. Gopiraman and K. Subramanian, *Prog. Org. Coat.*, 2014, **77**, 836–844.
30 S. Kunjukunju, A. Roy, M. Ramanathan, B. Lee, J. E. Candiello and P. N. Kumta, *Acta Biomater.*, 2013, **9**, 8690–8703.

31 M. Stern and A. L. Geary, *J. Electrochem. Soc.*, 1957, **104**(1), 56–63.
32 X. Yu, Z. W. Ning, M. Hua, C. B. Wang and F. Z. Cu, *J. Mater. Chem. B*, 2013, **1**, 4773–4780.
33 Y. J. Lu, P. Wan, B. C. Zhang, L. L. Tan, K. Yang and J. X. Lin, *Mater. Sci. Eng., C*, 2014, **43**, 264–271.
34 R. C. Zeng, Z. G. Liu, F. Zhang, S. Q. Li, H. Z. Cui and E. H. Han, *J. Mater. Chem. A*, 2014, **2**, 13049–13057.
35 G. S. Wu, J. M. Ibrahim and P. K. Chu, *Surf. Coat. Technol.*, 2013, **233**, 2–12.
36 H. Tamai, K. Igaki, E. Kyo, K. Kosuga, A. Kawashima, S. Matsui, H. Komori, T. Tsuji, S. Motohara and H. Uehata, *Circulation*, 2000, **102**(4), 399–404.
37 X. M. Li, Y. G. Wang, J. M. Chen, Y. N. Wang, J. B. Ma and G. L. Wu, *ACS Appl. Mater. Interfaces*, 2014, **6**, 3640–3647.
38 X. Z. Ding and P. Yao, *Langmuir*, 2013, **29**(27), 8636–8644.
39 P. M. Kharkar, A. M. Kloxin and K. L. Kiick, *J. Mater. Chem. B*, 2014, **2**, 5511–5521.
40 A. Santos, M. S. Aw, M. Bariana, T. Kumeria, Y. Wang and D. Losic, *J. Mater. Chem. B*, 2014, **2**, 6157–6182.
41 C. M. Xie, X. Lu, K. F. Wang, F. Z. Meng, O. Jiang, H. P. Zhang, W. Zhi and L. M. Fang, *ACS Appl. Mater. Interfaces*, 2014, **6**, 8580–8589.
42 G. Fotakis and J. A. John, *Toxicol. Lett.*, 2006, **160**, 171–177.
43 H. M. Wong, K. W. K. Yeung, K. O. Lam, V. Tam, P. K. Chu and K. L. K. Cheung, *Biomaterials*, 2010, **31**, 2084–2096.
44 W. H. Ma and Y. Z. Zhang, *Chin. J. Tissue Eng. Res.*, 2014, **18**, 432–439.
45 J. C. Zhou, X. Z. Zhang, Q. Li, Y. Liu, F. N. Chen and L. Q. Li, *J. Mater. Chem. B*, 2013, **1**, 6213–6224.
46 Z. L. Wei, P. Tian, X. Y. Liu and B. X. Zhou, *Colloids Surf., B*, 2014, **121**, 451–460.